AD-A159 507 THE BALLISTIC RESEARCH LABORATORY FLASH X-RAY COMPUTED 1/1
TOMOGRAPHY FACILIT (U) ARMY BALLISTIC RESEARCH LAB
ABERDEEN PROVING GROUND MD C K ZOLTANI ET AL SEP 85
UNCLASSIFIED BRL-TR-2671 F/G 14/2 NL

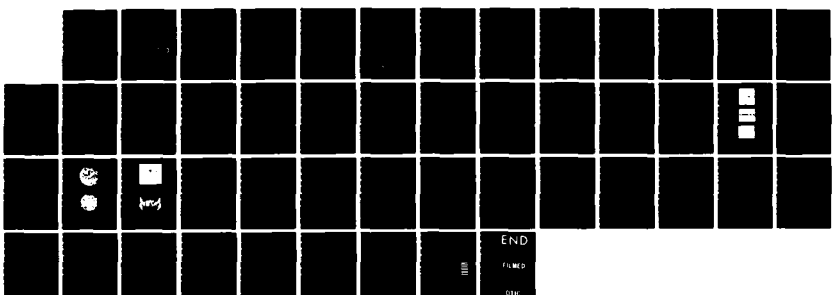

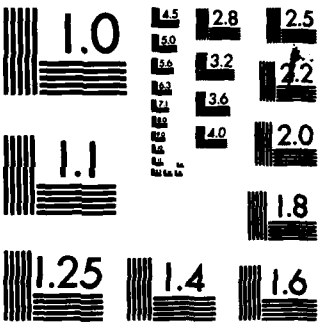

MICROCOPY RESOLUTION TEST CHART
NATIONAL BUREAU OF STANDARDS-1963-A

(2)

AD

US ARMY MATERIEL COMMAND

TECHNICAL REPORT BRL-TR-2671

AD-A159 507

THE BRL FLASH X-RAY COMPUTED TOMOGRAPHY FACILITY FOR MICROSECOND EVENTS

Csaba K. Zoltani
Kevin J. White
Frank A. Di Bianca

September 1985

US ARMY BALLISTIC RESEARCH LABORATORY
ABERDEEN PROVING GROUND, MARYLAND

Destroy this report when it is no longer needed.
Do not return it to the originator.

Additional copies of this report may be obtained from the National Technical Information Service, U. S. Department of Commerce, Springfield, Virginia 22161.

The findings in this report are not to be construed as an official Department of the Army position, unless so designated by other authorized documents.

The use of trade names or manufacturers' names in this report does not constitute indorsement of any commercial product.

UNCLASSIFIED

SECURITY CLASSIFICATION OF THIS PAGE *(When Data Entered)*

REPORT DOCUMENTATION PAGE		READ INSTRUCTIONS BEFORE COMPLETING FORM
1. REPORT NUMBER BRL-TR-2671	2. GOVT ACCESSION NO. AD-A159507	3. RECIPIENT'S CATALOG NUMBER
4. TITLE *(and Subtitle)* The Ballistic Research Laboratory Flash X-Ray Computed Tomography Facility For Microsecond Events.		5. TYPE OF REPORT & PERIOD COVERED Final 6. PERFORMING ORG. REPORT NUMBER
7. AUTHOR(s) Csaba K. Zoltani Kevin J. White Frank A. Di Bianca		8. CONTRACT OR GRANT NUMBER(s)
9. PERFORMING ORGANIZATION NAME AND ADDRESS U.S. Army Ballistic Research Laboratory Attn: AMXBR-IBD Aberdeen Proving Ground, MD 21005-5066		10. PROGRAM ELEMENT, PROJECT, TASK AREA & WORK UNIT NUMBERS 1L161102AH43
11. CONTROLLING OFFICE NAME AND ADDRESS U.S. Army Ballistic Research Laboratory Attn: AMXBR-OD-ST Aberdeen Proving Ground, MD 21005-5066		12. REPORT DATE September 1985 13. NUMBER OF PAGES 48
14. MONITORING AGENCY NAME & ADDRESS*(if different from Controlling Office)*		15. SECURITY CLASS. *(of this report)* Unclassified 15a. DECLASSIFICATION/DOWNGRADING SCHEDULE

16. DISTRIBUTION STATEMENT *(of this Report)*

APPROVED FOR PUBLIC RELEASE; DISTRIBUTION UNLIMITED.

17. DISTRIBUTION STATEMENT *(of the abstract entered in Block 20, if different from Report)*

18. SUPPLEMENTARY NOTES

19. KEY WORDS *(Continue on reverse side if necessary and identify by block number)*

Computed Tomography
Microsecond Tomography
Flash X-Ray
Solid State Detector

20. ABSTRACT *(Continue on reverse side if necessary and identify by block number)*

A new technique using multiple flash x-ray sources for the determination of cross-sectional density profiles of rapidly translating or dynamically deforming objects is presented. The method, an extension of the concepts of medial tomography, allows stop-action survey of events with time constants at the low end of the microsecond range, making it suitable for problems of ballistic research and materials proof testing. This report discusses the design, the components, the capabilities, as well as the system studies which led up to the

DD FORM 1 JAN 73 1473 EDITION OF 1 NOV 65 IS OBSOLETE

UNCLASSIFIED

SECURITY CLASSIFICATION OF THIS PAGE *(When Data Entered)*

Abstract (Cont'd):

configuration which is under construction at BRI..

TABLE OF CONTENTS

LIST OF FIGURES

1. INTRODUCTION

A new technique using multiple flash x-ray sources for the determination of cross-sectional density profiles of rapidly translating or dynamically deforming objects is presented. The method, an extension of the concepts of medical tomography, allows stop-action survey of events with time constants at the low end of the microsecond range, making it suitable for problems of ballistic research and materials proof testing.

The rapidity of ballistic events places severe requirements on the design of a computed tomography facility. In addition to the short time available for data registration, spatial resolution in the millimetre range and a density resolution better than one percent is required. Also, the x-ray beam has to be energetic enough to traverse at least two centimetres of a high atomic number material such as steel with the emerging beam having a signal to noise ratio favorable for good image quality. Such energy and dosage levels are obtainable from commercial flash x-ray units rated in the megavolt range.

In fourth-generation conventional CT systems, the source is rotated around a stationary object with the transmitted radiation recorded by a stationary ring of detectors. Data acquisition times of a few seconds are common. With time constants of the observed scene of the order of microseconds, mechanical motion of the source is no longer feasible and another means of obtaining the transmission profiles must be considered.

The first practical approach to CT of moving objects resulted in the building of the Dynamic Spatial Reconstructor of the Mayo Clinic. By means of gating, and using 28 separate thermionic x-ray sources, pictures of acceptable quality of the beating heart have been obtained.[1] In view of the long pulse width (around 300 microseconds) of the thermionic x-ray sources, this method is not suitable for ballistic applications.

Scanning electron beam systems, such as the Imatron C-100 cine-CT scanner,[2] where an electron beam is magnetically deflected along a circular anode ring generating an electronically movable x-ray source, show promise of higher temporal resolution but as yet, due to problems with heating of the anode, are limited to lower energies and longer time scales than those required for ballistic applications.

A solution to the problem of generating all the transmission profiles needed in a few microseconds is possible by the use of simultaneously-triggered multi-source arrangement. Ideas along these lines were advanced by

---

[1] J.H. Kinsey, R.A. Robb, E.L. Ritman, E.H. Wood, "The DSR- a High Temporal Resolution Volumetric Roentgenographic CT Scanner," Herz, Vol.5, #3, pp. 177-188, 1980.

[2] D.W. Farmer, M.J. Lipton, C.B. Higgins, "Cine-CT Captures the Beating Heart," Diagnostic Imaging, Vol.6, pp. 54-58, 1984.

Trimble and Aseltine[3] who developed a six source sequentially-fired radiographic facility.

A recently completed feasibility study by two of the present authors[4] has shown that industrial quality tomographic data of events having time constants in the microsecond range is indeed possible. There, it was demonstrated that on mock-ups of ballistic interest, typically objects up to 50 cm in diameter and having constituents consisting of Si, C, N, O, a 1 MV source would provide transmitted photons adequate in number and energy to assure a favorable signal- to-noise ratio at the detector and thus an acceptable tomographic reconstruction. Here, we discuss and expand on these findings and detail the design, the components, the capabilities, as well as some of the system studies which led up to the configuration which is under construction and scheduled for completion in the near future.

2. LAYOUT OF THE FACILITY

A schematic diagram of the tomographic layout is given in Figure 1. The twenty-one sources and detector arrays (which can be either medical film-screen cassettes or solid state detectors) are arranged in a 360° arc about the object. This configuration has the advantage over the previous design[4] of being more compact, allowing for both more sources and a smaller source-to-object distance. As a consequence, a larger dose will be received by the object and the detector, increasing the sensitivity. There are, however, disadvantages. Shielding of the detectors from unwanted scattered and punch-through radiation will be slightly more difficult. Details of the layout are given in Table 1.

Table 1. System Parameters

Scan diameter	25 cm
Beam thickness	2-10 mm
Number of sources	21
Source to object distance	2.10 m
Focal spot size	1-5 mm
Pulse width	25 ns
Source voltage	1 MV
Dose	65 mR @ 1 m
Source to detector distance	3.78 m
Magnification	variable

The system can also be used to obtain conventional radiographs. The collimator, which determines the slice thickness (2 to 10 mm), can be removed or widened to obtain 21 radiographs. The sources could be fired sequentially

---

[3] J. Trimble, C.L. Aseltine, "Flash X-Ray and Cineradiography at 100 000 Fps," May 1983, ARBRL-TR-02491, Aberdeen Proving Ground, MD, ADA 129090.

[4] C.K. Zoltani, K.J. White, R.P. Kruger, "Result of Feasibility Study on Computer Assisted Tomography for Ballistic Applications," August 1983, ARBRL-TR-02513, Aberdeen Proving Ground, MD, ADA 133214.

in time for cine-radiographic data. Additionally, they could be fired in pairs giving 10 sets of nearly orthogonal (85.7°) radiographs. Sources could also be fired in adjacent pairs to yield stereographic images. A potential problem exists with this setup. The focal spot size of conventional high-voltage flash tubes is 5mm. The arrangement shown in Figure 1 has a relatively large object-to-screen/source-to-object ratio. This will produce radiographs with large penumbras with potentially blurred images. This can be improved by using a demountable anode tube where smaller focal spots can be realized. An alternative solution is to decrease the object-to screen distance. The detector screens are moved onto a smaller circle, in Figure 1. In this position only five radiographs will be produced by firing x-ray units marked No. 1 through No. 5. Alternative configurations are also possible that will give more than 5 radiographs but with some sacrifice of resolution.

The layout discussed up to now allows the smallest object to source and object to detector distances. We now discuss the advantages of this layout, hereafter referred to as System III, see Figure 1 in comparison to a previous and also viable approach, described in Reference 4, called System II and which is shown in Figure 2.

3. SYSTEMS ANALYSIS

3.1 Background

A complete derivation of the equations which describe the most compact geometries for Systems II and III is given in the Appendix A. These geometrical equations are plotted in Figure 3 for a 25 cm scan circle diameter. d_S is the source-to-object center distance and d_D is the detector-to-object center distance.

3.2 Comparison of Systems II and III

It can be seen directly that System III is always more compact than System II. For example, with a magnification of 1.5 and 21 beams, the source-to-detector distance for System II is 7.5 m whereas for System III it is only 5.0 m. The smaller size of System III allows the substructure supporting the sources and detectors to be smaller and less costly. It further allows a higher x-ray intensity at the detector giving lower image noise and better contrast resolution.

Because in System III the sources cover a full 360 degrees, a more uniform sampling and a balanced slice thickness will be obtained. In fact, System II, which is constrained to have a source arc of less than 180 degrees cannot yield a mathematically complete reconstruction. A complete reconstruction for a fan beam geometry requires a source arc of 180 degrees plus the fan angle.

The final advantage of System III relates to the fact that it has nearly opposing detectors. By shifting each detector clockwise (or counterclockwise) by one-quarter of a detector cell width, opposing fan beams are displaced laterally by one-half of a cell width relative to each other. This

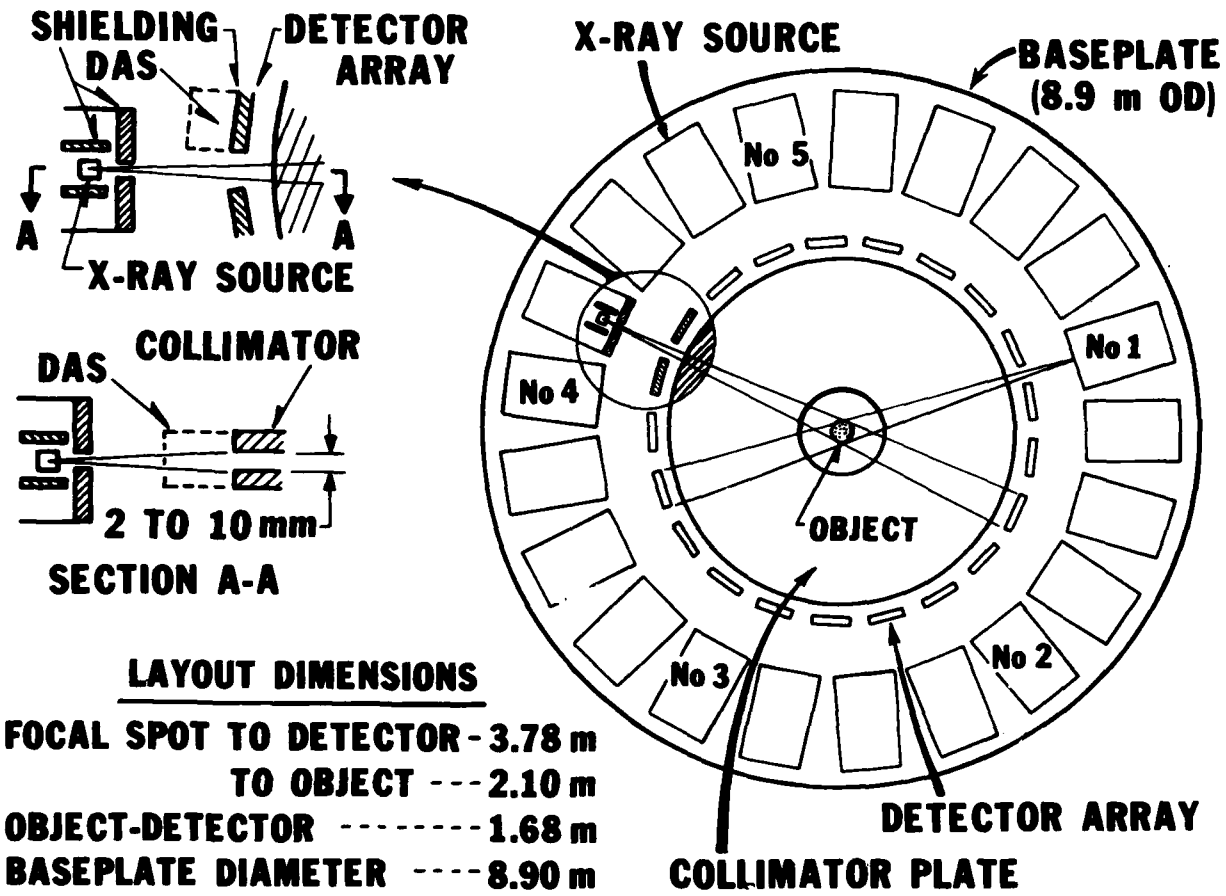

Figure 1. Layout of the Facility

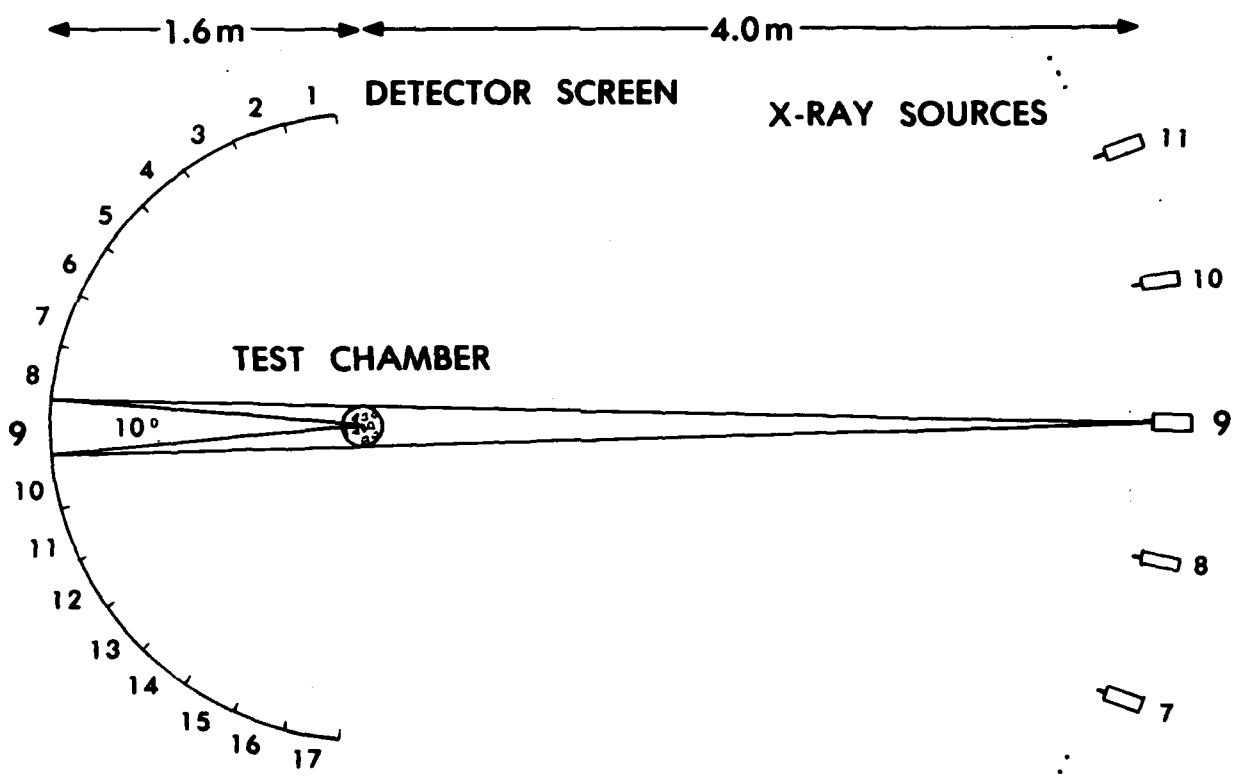

Figure 2. System II Design.

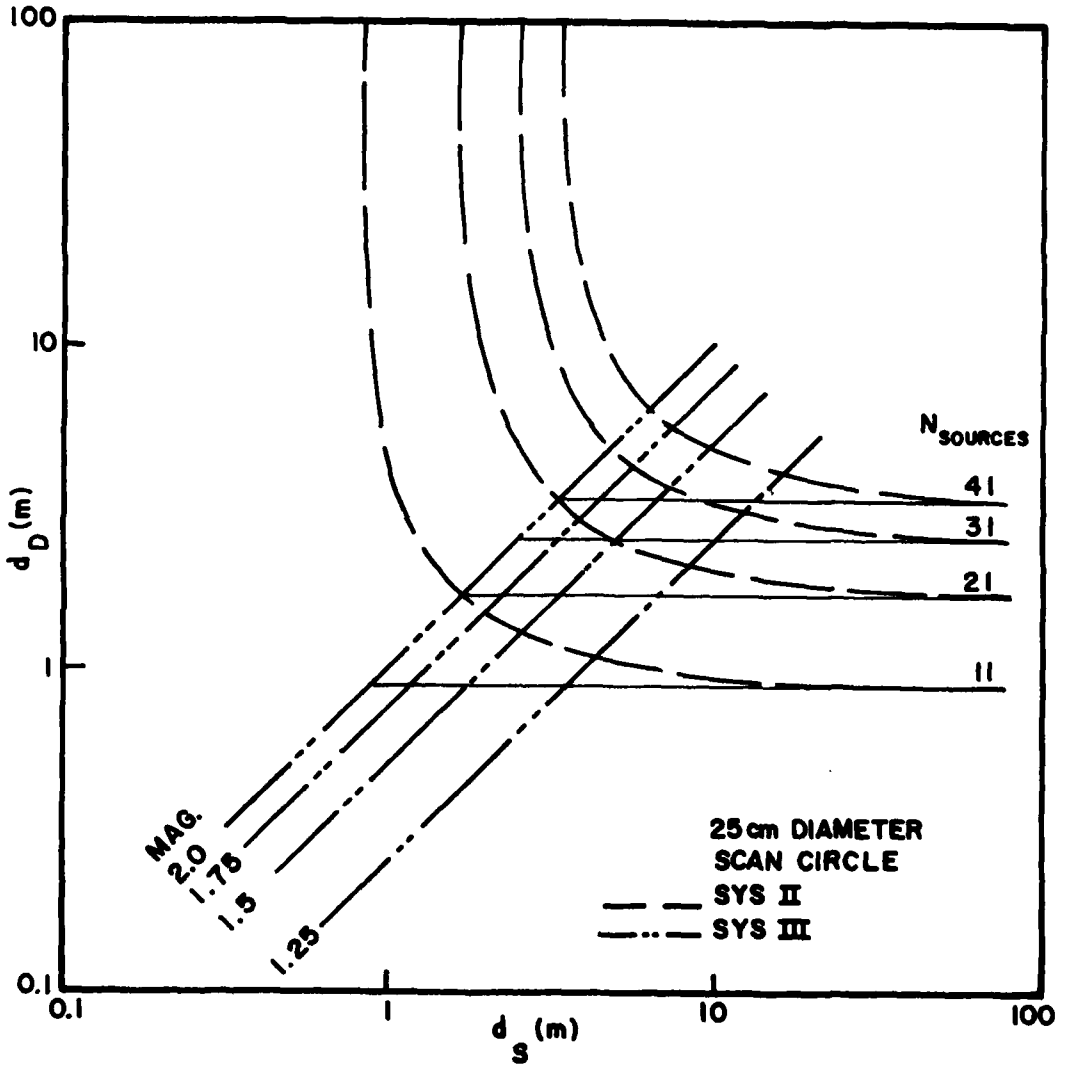

Figure 3. Detector Distance Versus Source Distance For System II and III Geometries.

effectively doubles the sampling frequency (see sec. 3.4.1.1) allowing higher resolution and reduced aliasing.[5]

Advantages of System II are its ability to incorporate magnifications in excess of 2 more easily than System III and a slightly lower shielding requirement resulting from the larger effective separation between tubes and detectors compared to System III. On balance however, the advantages of System III significantly outweigh those of System II.

3.3 Electronic Detector Arrays

The basic constraints on an electronic detector array for the BRL Flash CT System are similar in some respects and different in others to those of modern medical CT scanners. The x-ray exposure levels per view and the expected dynamic ranges are similar; however the total number of views is 30-50 times higher for medical CT. The object size ranges and the required slice thicknesses are also similar.

On the other hand, the required spatial and contrast resolutions are lower and there is no limit on how fast the data must be read out even though the x-ray pulse time is five orders of magnitude faster than medical CT. Also, there can be several centimetres of steel present in objects of military interest. The major difference, and challenge from the design viewpoint, is the much higher energy x-ray beam spectrum in the flash CT.

The higher energy x-ray spectrum has several ramifications. First, one needs much thicker scintillator crystals to absorb the incident radiation and to prevent increased noise from x-ray photons which punch through the scintillator and then interact in rear-mounted photodiodes. Since most of the lower energy photons will be absorbed via photoelectric interactions while most of the higher energy x-rays will produce Compton scattering, the latter resulting in high-energy outgoing x-ray photons, these scattered x-rays can then interact in adjacent detectors to blur the resolution.

As a result of all these considerations, the first electronic CT detectors will use cesium iodide scintillators as a compromise in atomic number, density and radiant efficiency (light output). Based on the results obtained with this scintillator, future electronic detectors may use alternative materials.

The anticipated detector design parameters are listed in Table 2 (taken from the BRL detector specifications).

---

[5] R.A. Brooks, G.H. Glover, A.J. Talbert, R.L. Eisner, F.A. DiBianca, "Aliasing- a Source of Streaks in Computed Tomograms," J. Comput. Assist. Tomography, Vol. 3, #4, 1979, pp. 511-518.

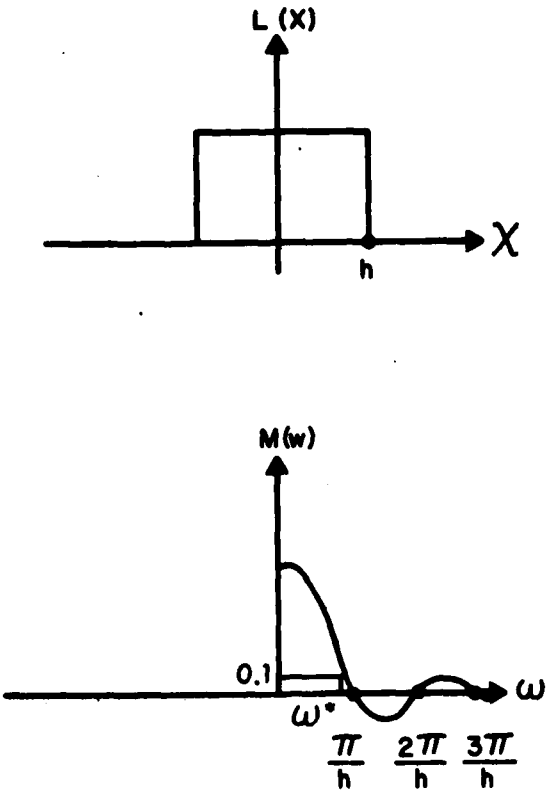

4a. Rectangular Line Spread Function and Corresponding Modulation Transfer Function.

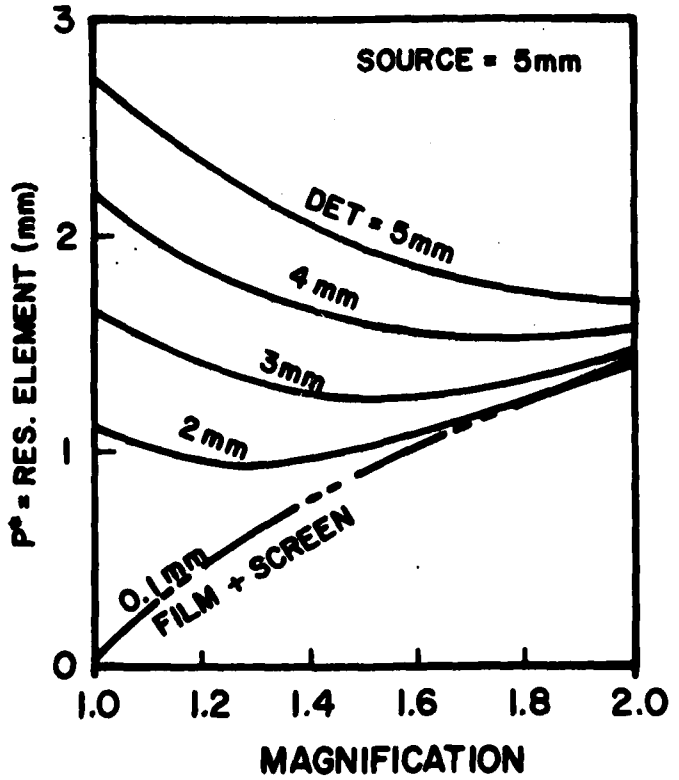

Figure 4b. Spatial Resolution Versus Magnification for Various Detector Sizes

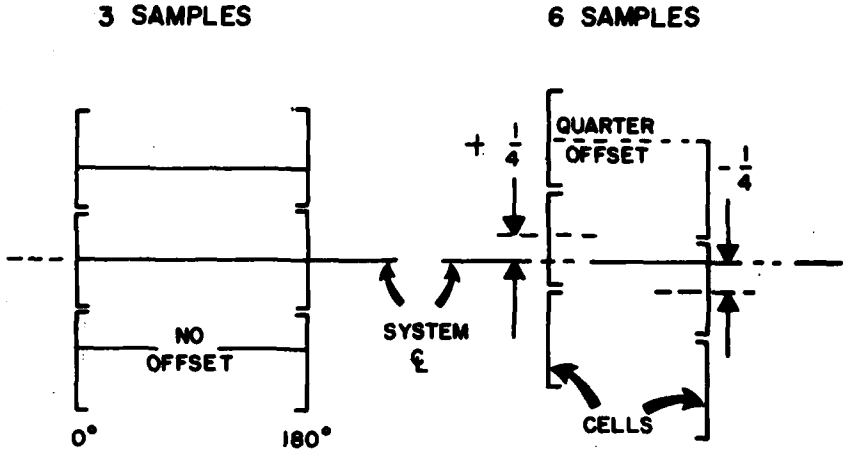

Figure 4c. Schematic Representation of Zero and Quarter-Offset of the Detector Cells (Digitization Cells for Film).

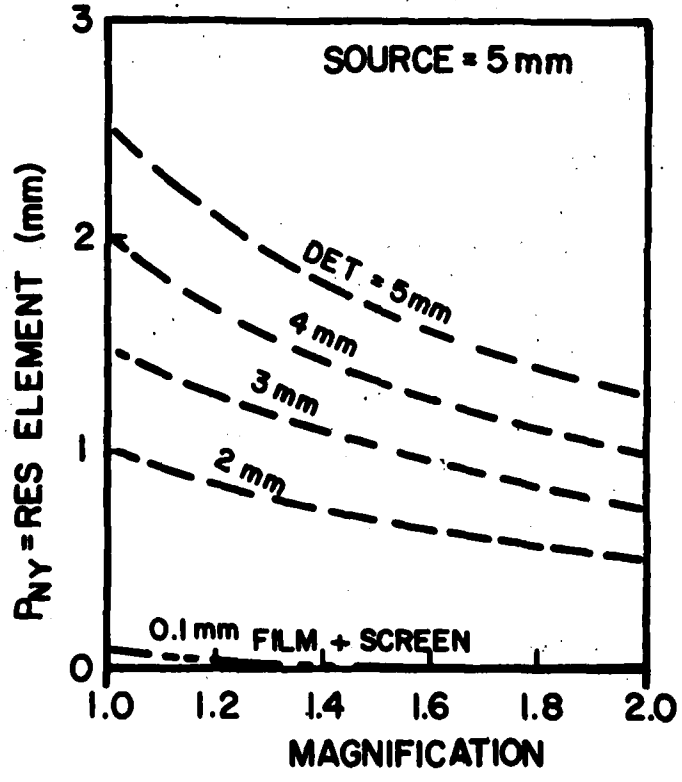

Figure 4d. Effective Nyquist Resolution Element Versus Magnification for Various Detector Sizes.

Table 2. Detector System Characteristics

Detector material	Cesium iodide (Tl)
width by height	0.302 by 2.5 cm
length	2 cm
radiation efficiency	> 12 %
Photodiode	CT-type, less than 5% variation in radiant sensitivity over active area
Collimator plates	Tungsten
dimension	0.05 x 3.0 x 14.5 cm
Performance parameters	
output signal	average over 5×10^{-16} coul/200 keV. x-ray absorbed in scintillator
optical crosstalk	< 2 % between adjacent cells
non-linearity	< 2 %

3.4 System Characteristics

The image quality of the flash CT system is characterized by three principal parameters: static spatial resolution, dynamic spatial resolution and contrast resolution. These parameters refer respectively to the system's ability to resolve detailed structure, to freeze or avoid blurring in highly dynamic events and to discriminate between two adjacent areas which differ slightly in x-ray attenuation coefficient.

3.4.1 Static Spatial Resolution

For a CT scanner, there are two stages at which the spatial resolution should be evaluated. These stages are after the view projection data have been accumulated and after the final image has been reconstructed.

3.4.1.1 Projection Resolution

The spatial resolution of an imaging system can be characterized using the modulation transfer function $M(\omega)$, where ω is the spatial frequency in units of length^{-1} and represents the ratio of the amplitude of the output signal to that of a sinusoidal input signal or object of frequency ω. The normalization of $M(\omega)$ is usually defined such that $M(0) = 1$.

The modulation transfer function (also referred to as the MTF) equals the modulus of the Fourier Transform of the corresponding "shape function" $L(x)$ which can be the source shape, the detector response shape, a combination of the two, or any other spatial shape function. Thus,

$$M(\omega) = \left| \int_{-\infty}^{\infty} L(x) \exp(-i\omega x)\, dx \right| . \qquad (1)$$

Since the combined effect of two shape functions is obtained by convoluting the individual shape functions, it follows from the above equation

that the combined effect of two MTF's is obtained by multiplying the individual MTF's,(see Reference 6). More specifically, the total MTF of the source and detector is the product of the source and detector MTF's after each is scaled to the object plane using the system magnification m, which is the ratio of the image size to object size.

Given a rectangular shape function L(x) with half-width h, the local (unscaled) MTF is

$$M(\omega) = \text{sinc} (h \omega) \qquad (2)$$

where sinc (x) = sin (x) / x. Plots of L(x) and M(ω) are given in Figure 4a. The total MTF at the object plane resulting from the combination of rectangular source and detector shapes is then (Reference 7):

$$M_{tot}(\omega) = \text{sinc}[(m-1)/m\ h_{so}\ \omega]\ \text{sinc}[1/m\ h_{det}\ \omega] \qquad (3)$$

where the source and detector half-widths are h_{so} and h_{det} respectively. The limiting spatial resolution of the imaging system is defined here as the frequency at which the system MTF drops off to 0.1, i.e. that frequency, ω, where the output amplitude drops off to 10% of the input amplitude. Thus, as shown in Figure 4a, we must find ω* for a value of M = 0.1. The limiting angular spatial frequency ω* can now be used to determine a limiting spatial resolution p* as

$$p^* = 1/ \omega^*. \qquad (4)$$

The equation for M_{tot} is transcendental however, i.e., ω cannot be found in terms of M_{tot} so the limiting value of ω (ω*) is found by iteration using the Method of False Position and the result is indicated in Figure 4a. p* corresponds to the sampling aperture of the system and is shown in Figure 4b for a 5 mm source width and several values of detector widths and magnifications.

Another limiting resolution element p_{Ny} can be defined corresponding to the Nyquist sampling frequency f_{Ny} of the detector[8]:

$$p_{Ny} = 1 / f_{Ny} = 2\ h_{det} \qquad (5)$$

If objects smaller than (i.e., frequencies higher than) the Nyquist frequency are imaged, aliasing artifacts (streaks) usually result.

In using p_{Ny}, two factors must be considered. First, the equation must be scaled to the object plane. Secondly, the detector offset from the system

---

[6] T.H. Newton, D.G. Potts, Radiology of the Skull and Brain. Technical Aspects of Computed Tomography, The C.V. Mosby Company, St.Louis, 1981.

[7] C.M. Coulam, The Physical Basis of Medical Imaging, Appleton-Century-Crofts, New York, pp. 60, 97, 1981.

[8] T.H. Newton and D.G. Potts, (ibid), p. 3931.

centerline must be taken into account (see Figure 4c). If zero offset is used, the opposing detector pairs will align and the Nyquist frequency will not change. If "quarter offset" is used, opposing fan beams will be offset by one-half the sampling distance and the Nyquist frequency will be doubled (Reference 5). The detectors in System III opposite one another are nearly one-quarter offset, resulting in a near-doubling of the Nyquist frequency. Combining the scaling and offset factors gives:

$$p_{Ny} = 2\ h_{det} / m \quad (\text{0 offset}) \tag{6}$$

$$p_{Ny} = h_{det} / m \quad (\text{1/4 offset}). \tag{7}$$

The variation of p_{Ny} with detector width and magnification is shown in Figure 4d. Inspecting Figs. 4b and 4d leads to several insights:

1. For magnifications only slightly less than two, there is little gain in p^* when small detector elements are used.

2. When the detector element is equal to (slightly smaller than) the source size, the optimum magnification is 2 (between about 1.6 and 2); but when a very high resolution detector such as screen film is used, the resolution continues to improve down to very low magnifications. These conclusions are straightforward results of Equation 3.

3. A quarter-offset alignment should theoretically help to reduce aliasing and thereby allow higher spatial resolution. In practice, however, the deleterious effects from the severely limited number of views (view aliasing) may eliminate most of this benefit.

4. As magnification increases, p_{Ny} continually improves since the sampling distance at the object plane continually decreases.

As a check on the equations, the theoretical values for limiting spatial resolution were calculated and compared to published values (Reference 9) for two commercial CT scanners and found to agree within 15-20 %. These machines are not view limited as reconstructed images are formed from hundreds of projections rather than the 21 used in the BRL system. However one expects the CT resolution of the BRL design to be degraded from the theoretical resolution by more than this amount. On the other hand, the projection resolution of the BRL machine should be close to the theoretical estimates.

3.4.1.2 Image Resolution

The image resolution is more difficult to obtain than the projection resolution. The image resolution is always degraded from the projection resolution by an amount which depends on the number of views available and on the algorithm used for reconstruction. Thus, the final resolution can be

---

[9] Anonymous, "CT/T 8800 Technology Brochure, General Electric Medical Systems," 1979; "CT 9800 Evaluation Criteria," General Electric Medical Systems, 1981.

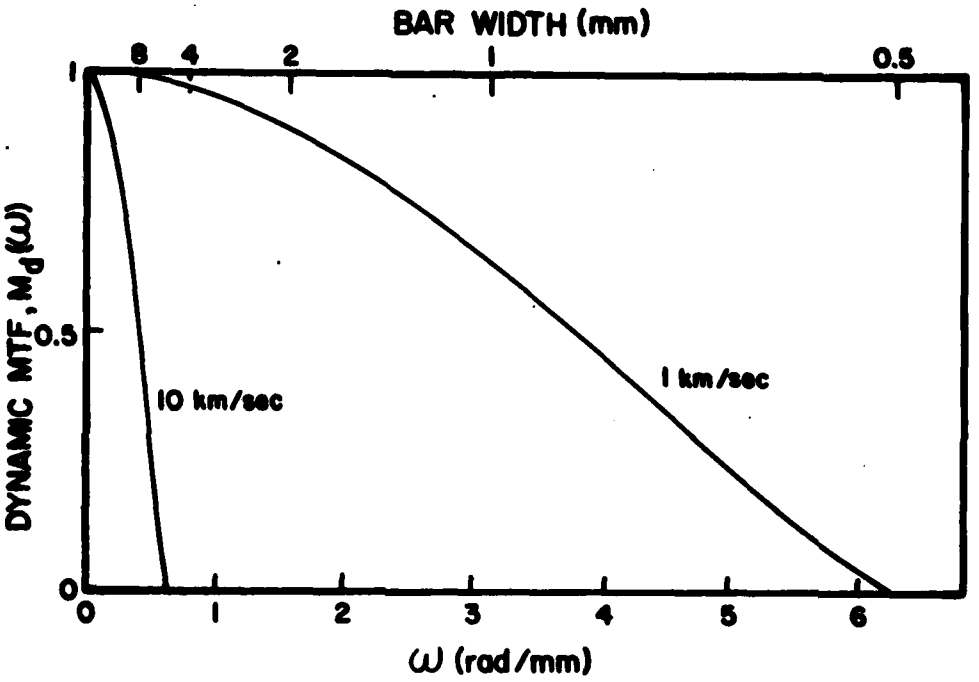

Figure 5. Dynamic Modulation Transfer Function Versus Angular Frequency and Bar Width.

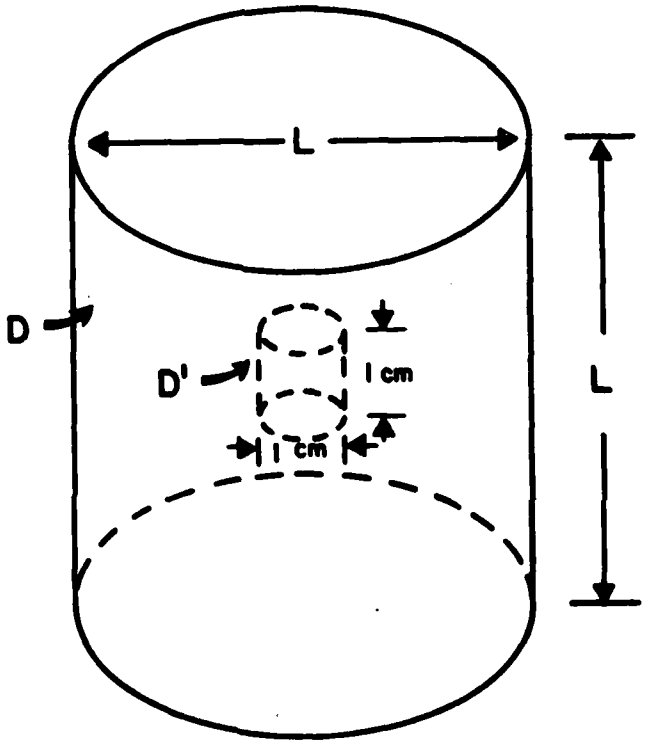

Figure 6. Schematic of Water Phantom Used for Projection and CT Contrast Resolution Determination.

determined only with the actual reconstruction algorithm operating on real or accurately-simulated data and is not given here.

3.4.2 Dynamic Spatial Resolution

The dynamic spatial resolution refers to image blurring from object motion perpendicular to the beam direction during the x-ray pulse and can be characterized by an appropriate MTF. The effect of such object motion can be expressed as a convolution of the system's static line spread function (LSF) with a dynamic LSF. The shape of the dynamic LSF will be the same as that of the x-ray intensity-versus-time curve but having a width equal to the object motion during the x-ray pulse. It is convenient to determine the MTF corresponding to the motion blurring so that the total system MTF including motion can be expressed as the product of the static and dynamic MTF's.

Since the x-ray pulse time is approximately 25 nsec, the corresponding dynamic MTF for projection radiography is virtually perfect (flat with a value of one) for all spatial frequencies of importance in ballistics studies. However, for CT operation one cannot assume that all 21 sources will fire simultaneously. Calling the time over which all tubes discharge t and the velocity of the moving structures v, the dynamic MTF M_d is given by:

$$M(\omega)d = \text{sinc}(vt\omega/2). \qquad (8)$$

Assuming that t = 1 microsec and v = 1 and 10 km/sec yields a dynamic MTF as shown in Figure 5. At velocities of up to 1 km/sec there is little loss of resolution for objects larger than 2 mm.

3.4.3 Contrast Resolution

As was done for spatial resolution, one can also consider the contrast resolution in each projection as well as that of the final reconstructed CT image. Both are treated in this section.

3.4.3.1 Projection Contrast Resolution

To calculate the contrast resolution in each projection, we consider a uniform water phantom of thickness L containing a small object having the same mass attenuation coefficient as water but a different electron density. The object is taken to be a cylinder with a diameter of 1 cm, 1cm in length and with a density slightly different from water. This configuration is shown in Figure 6.

The projected density contrast C is defined as the fractional difference in the density of the small cylinder D and the background D'.

$$C = (D - D') / (.5 \times (D + D')). \qquad (9)$$

The x-ray energy spectrum was calculated on an IBM-PC computer with the program XRSPEC which determines the bremsstrahlung and characteristic spectra for an arbitrary voltage and current waveform. The waveforms for the 1 MV flash x-ray source used at BRL were obtained by scaling the data in Figure

2.32 of Reference 10 to a voltage of 1 MV. The program also calculates the exposure for a given electron charge transported in the x-ray tube (called mAs or current-time product when the current and voltage are constant).

The detector was modeled as a cesium iodide crystal array with a 2 cm thickness. The signal was taken as the total energy absorbed in the scintillator excluding reabsorption of scattered x-rays. The image noise was considered to arise exclusively from the statistical fluctuations in the absorbed energy. Furthermore, the x-ray flux was scaled to agree with experimental measurements taken with a 4 mm focal spot flash x-ray tube and then adjusted for the 2.1 m source-to-center distance.

The contrast resolution C* is defined as the threshold density contrast which produces a signal-to-noise ratio of 8. This value is based on the typical results of observer studies in medical x-ray imaging and represents the smallest perceivable signal-to-noise ratio. As an example, if the density contrast of two objects can be resolved by an observer then the difference in the grey scale value of the two objects divided by the average noise in the images will be 8, or larger. For a single x-ray pulse, the resulting projection contrast resolution is given in Table 3.

Table 3. Calculated projection contrast resolution versus phantom diameter.

L(cm)	C*(%)
01	0.7
10	1.4
20	2.7
30	5.3

3.4.3.2 Image Contrast Resolution

The contrast resolution of the final CT image may be estimated by two different methods given in this section. The first method uses the projection contrast resolution calculated in the previous section, while the second method involves scaling published data from a medical CT scanner.[11] Since the latter data were obtained with a 16.5 cm diameter water phantom and a 1 cm slice thickness, the same values are used here.

Assuming that the CT contrast resolution scales with the total image noise (i.e., with the inverse square root of the total number of x-ray photons detected in all views) and performing a log-log interpolation of the data in Table 3 to an L value of 16.5 cm giving C* = 2.3. Since in the BRL System III there are 21 projections,

---

[10] F. Jamet, G. Thomer, Flash Radiography, Elsevier Scientific Publishing Co., Amsterdam, 1976.

[11] G. Cohen, F.A. DiBianca, "The Use of Contrast-Detail-Dose Evaluation of Image Quality in a Computed Tomographic Scanner," J. Comput. Assist. Tomography, Vol.3, #2, pp. 189-195, 1979.

$$C_{CT}^{*} = 2.3/(21)^{1/2}\% = 0.5\ \%\quad \text{(method 1)} \tag{10}$$

For the second method, which also assumes that the contrast resolution varies inversely with the square root of the total number of x-ray photons detected, we begin by estimating the total radiation exposure delivered in a 21 view CT scan. Summing the radiation exposure along the lines from each source position to a point on the phantom surface and attenuating by the appropriate chord lengths through the phantom gives an estimated total exposure of 233 mR. Then the CT contrast resolution can be estimated from

$$C_{CT}^{*} = k\ (\ R\ h\ )^{-1/2} \tag{11}$$

where R is the exposure, h is the slice thickness and k is the unknown proportionality constant. Using the values from Reference 11, namely C* = 0.16 %, R = 5000 mR and h = 1 cm, we determine k and then obtain for the BRL flash CT system

$$C_{CT}^{*} = 0.8\ \%\quad \text{(method 2)}. \tag{12}$$

Considering the widely differing approaches and assumptions (except for the basic assumption related to the total x-ray detection), many of which are only approximations, used to obtain these estimates of CT contrast resolution, the agreement between the two methods is rather remarkable. These estimates lead us believe that the BRL flash CT scanner will have an actual contrast resolution near 1% for 1 cm diameter pins in a 16.5 cm diameter water phantom with a 1 cm slice thickness. The above analysis does not evaluate deleterious effects of the artifacts expected in the BRL system, for example artifacts due to limited number of views.

4. EXPERIMENTAL STUDIES

4.1 Background

Previous studies[4] on the feasibility of a ballistic tomography system were concerned with the quality of a cross-sectional image produced with a limited number of views or projections. Since between 15 and 25 were considered to be the maximum practical number of views, the impact of this limitation on the image was considered to be the most important aspect of the study. Consequently, the rest of the experimental set-up was idealized so as to minimize other problems. An essentially monochromatic source was used along with a well collimated source and detector so that scattering was minimized. A parallel-beam geometry was also used which simplified the algorithm. As is seen in Figure 1, the real system is somewhat more complicated. The flash x-ray source required to record the event in the microsecond time frame is not monochromatic but has a bremsstrahlung spectrum starting at low energies and extending up to the maximum discharge voltage which can be as high as 1 MV. Since the source is a single pulse system the dose output is limited and cannot be integrated in time. The collimation will not be ideal with a fan beam geometry and there will be a scattering contribution to each projection. The focal spot size for some flash x-ray systems can be as large as 5 mm. This will lead to a blurring of the image on each projection. The fan beam geometry will require a modified algorithm. Moreover, the radiation field produced by the flash x-ray source must be uniform over the object or, at least, reproducible otherwise accurate

attenuation measurements will not be possible. The first detector that will be used will be medical x-ray film and intensifying screens, rather than a scintillator and photodiode detector. This avoids the necessity of having over 2000 individual scintillators and associated data acquisition equipment. It also allows for the possibility of acquiring conventional two-dimensional radiographs of ballistic events. Also screen-film systems have high spatial resolution. However, film has a relatively limited dynamic range with respect to intensity and also does not have a wide range of linearity. The quantum detection efficiency is significantly less than the single crystal, photodiode array, leading to increased image noise and reduced contrast resolution. All of the above differences and uncertainties must be examined to determine the impact on the reconstructed image.

4.2 Single Channel Experiments

The source used in acquiring the data was a Hewlett-Packard 1 MV flash x-ray system. The propellant mock-up was placed inside a fiberglass chamber which, in turn, was located inside a lead container. Radiographs were taken through a horizontal slit in the lead container. A photograph of the side view of the propellant mock-up is shown in Figure 7a. A typical radiograph is seen in Figure 7b. An intensity profile of the radiograph is shown in Figure 7c.

This x-ray source delivers a nominal dose of 65 mR at a distance of 1 metre and a nominal focal spot size of 5 mm with a pulse duration of 25 nanoseconds. The focal spot size was measured by taking a radiograph of a tungsten plate and measuring the edge gradient as recorded on film. The dose was measured with a Radcal Model 1015C dosimeter which has an accuracy of 1%. The reproducibility of the source was determined by measuring the deviation of the dose over twenty one pulses. The standard deviation was measured to be 2%. The x-ray field uniformity was measured over a beam (plane) angle of 6° which covers almost any object of current interest. A medical film-screen cassette was placed at a distance of 2 metres from the source and was subjected to one pulse. The film was carefully developed in an automatic processor so as to avoid developing artifacts. The optical density of the film was measured with an X-Rite Model 301 densitometer with a resolution of ± 0.01 D. The optical density measured was in the linear region of the film (1.52 D). The variability of the optical density was less than ± 0.02 D (or ± 2% source intensity) over the area of the film corresponding to the 6° angle. The source was heavily shielded with lead plates. It was found that room scattering was a significant problem, giving unwanted scattered radiation at the detector. The shielding was required to reduce this problem. The average energy of the source was found by measuring the attenuation through several thicknesses of iron. The slope of the plot of ln(I) versus thickness yields an effective attenuation coefficient from which the average energy is obtained from cross section tables. Measurements made with both lead and iron yielded an average energy of 250 keV. The beam is hardened after passing through 0.64 cm of steel and the emerging radiation has an average energy of 600 keV.

The model seen in Figure 7a was mounted on an Ealing Model 35-2500 rotary stage. Eighteen projections were used in the reconstruction and the rotary stage was used to accurately position the object. The stage has an accuracy of better than one minute of arc and a deviation from horizontal plane of less

(a)

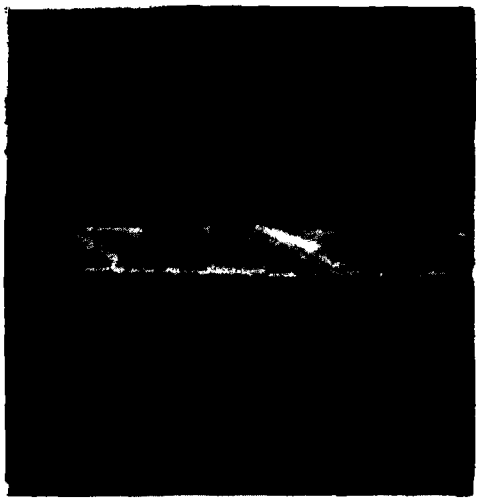

(b)

(c)

Figure 7a. Photograph of Propellant Mock-Up.
7b. Typical Radiograph.
7c. Intensity Profile of Radiograph.

than one arc minute. It can support a weight of up to 25 kg. For the projection data to be accurate, the axis of rotation must be perpendicular to x-ray radiation plane. To assure this, four positioning arrows were attached vertically to the rotation table. Radiographs were recorded of the four arrows at 0°, 90° and 180° intervals. The ends of the arrows should form a straight line on the radiograph. The rotating table was adjusted until this was achieved. An example of the radiograph is shown in Figure 7b. By having a fixed object in the radiograph, the axis of rotation can be determined from the 0° and 180° positions.

The detector used for these tests was a cassette of 3M Trimax 12 rare earth screens and XM film. This combination has a very high sensitivity with a slight loss in resolution over more conventional combinations. However, as was determined in Section 3.4.1.1, spatial resolution in the projection was not a major factor in the reconstructed image but signal-to-noise ratio was found to be very important. Additionally, the film response is more linear when the optical density is in the 0.7 to 2.5 region. This requires significant sensitivity for the intensifying screens. The question of linearity of the detector system remains. The system was calibrated using six plastic rods of different length, each one shielded with a lead sleeve so that scattering from one would not contribute a signal to the other. These were recorded on the same film with the projection data. Examination of the calibration data of optical density versus length indicated that the system was linear over the optical densities of interest hence recalibration of the data was not required.

4.3 The Data Set

Data were taken with a source-to-object distance of 3.31 metres, and with an object-to-detector distance of 0.223 metres. This configuration minimized the problem associated with the large (5 mm) focal spot size. The vertical height of the image represents the collimation window which was 25 mm. Optical density profiles of these data were acquired in two ways. First an Optronics microdensitometer was used employing a 0.2-mm sampling orifice to digitize the radiograph numerically. Six horizontal lines were averaged to produce a density profile over a height of 1.2 mm. These data were used in the reconstruction algorithm. An example of such a profile is given in Figure 7c. An Eyecom vidicon camera and a Comtal Vision One/20 image analyzer were also used to produce a series of profiles. Data were also taken with other object and detector distances, but they have not yet been used to reconstruct images.

5. RECONSTRUCTED IMAGES

5.1 The Algorithm

The number of views available from the BRL facility is only one tenth that of a conventional CT system. Consequently, considerable emphasis was placed during the design phase of the facility in arriving at the selection of a reconstruction algorithm which produces the least artifact-prone image. Computer experiments[4] showed that maximum entropy reconstructions were superior to conventional algorithms such as filtered back projection as far as

image quality was concerned. The higher quality though is bought at the expense of considerably-increased computer running time requirements.

Maximum entropy is based on several premises. This includes the notion that the image with the minimum information is the one represented by maximum entropy. Thus the object which transmits the minimum amount of information about itself has to be the one selected. Further, maximum entropy is valid without modification only when the object consists of isolated points. The maximum entropy image contains only the structure embodied in the data consequently leading to a minimization of the number of artifacts present in the image.

An already existing computer code, MENT, was chosen for the data reconstruction. A photograph of a mock-up along with the reconstructed image using the fan beam MENT algorithm are seen in Figure 8. The reconstruction gives a reasonable representation of the mock-up. MENT[12] is based on the concept of maximum entropy discussed at length in Reference 13, and involves the following steps: transmission data from the experiments are available in the form

$$G_{jm} = \iint f(x,y)dxdy \qquad (13)$$

where G_{jm} are the projection data, i.e., $\ln(I/I_o)$, the ratio of the measured to the incident radiation, and f(x,y) the attenuation in the region of the object under study. Since many functions satisfy this equation, a method was devised to select the function which came closest to picking out the attenuation observed. For this a second function, called the entropy is defined where

$$\zeta = \iint f(x,y)\ \ln(f(x,y)\ A\ )\ dxdy \qquad (14)$$

and a constrained optimization problem is solved. That is, one must find f which maximizes ζ subject to the constraints, i.e. the measured values. It is known that for a maximum to exist, Lagrange multipliers must exist such that f(x,y) is a stationary point of the Lagrangian. For this to be true, the functional derivative of the Lagrangian must be zero, leading to a system of nonlinear equations which are solved iteratively by the Gauss-Seidel technique. The solution converges to the image with the least amount of information, i.e., the one which has the fewest number of artifacts.

5.2 Results

In Figure 9, a reconstructed image of a mathematical mock-up consisting of a solid lucite rod in the center, an aluminum cylinder filled with water on the left, and a lucite tube filled with water on the right are shown. The

---

[12] G. Minerbo, "MENT: A Maximum Entropy Algorithm for Reconstructing a Source from Projection Data," Computer Graphics and Image Processing, Vol. 10, pp. 46-68, 1979.

[13] J. Skilling, "The Maximum Entropy Method," Nature, Vol. 309, pp. 748-9, 1984.

Figure 8. Mock-Up and Reconstructed Image.

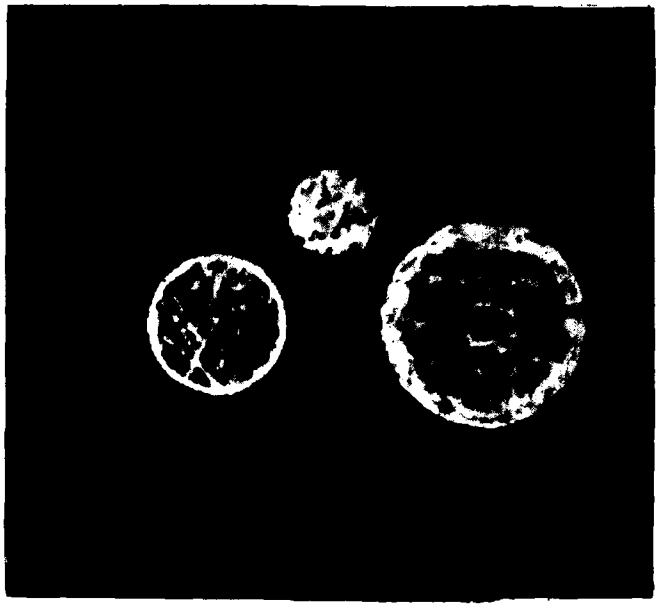

Figure 9. Density Resolution Capability of the System.

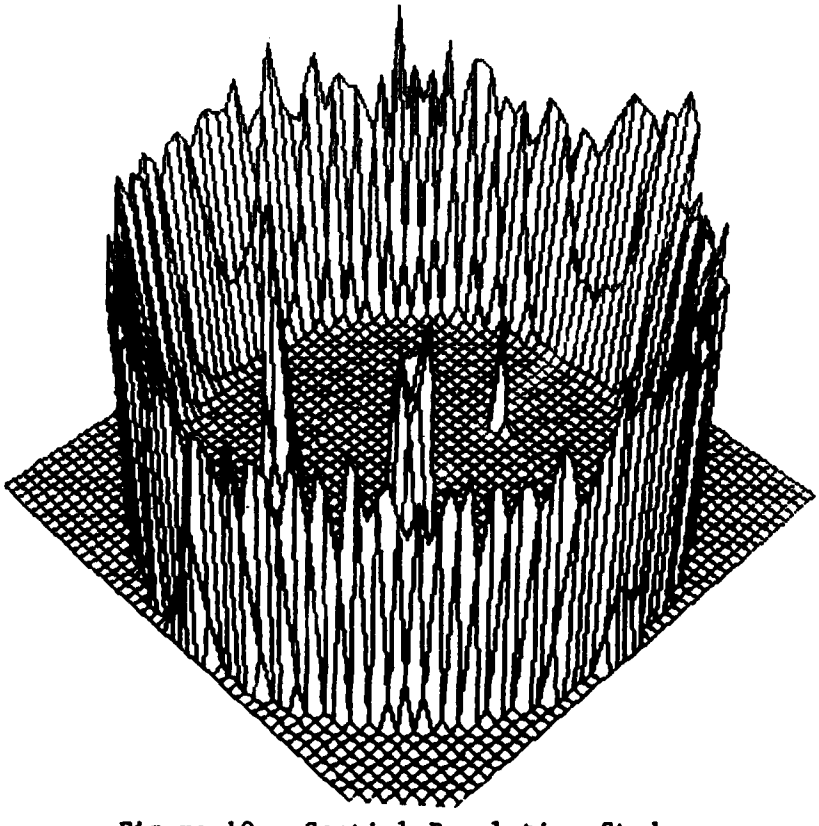

Figure 10. Spatial Resolution Study.

density difference between the lucite and the water is apparent. The spatial resolution capability of the system is illustrated in Figure 10 in a mock-up consisting of an aluminum tube containing lucite rods of 5, 3, and 1-mm in diameter. The 5 mm, and even the 3 mm and 1 mm rods are clearly visible. Reconstruction times are typically of the order of 8 minutes on a Cyber 76 computer.

6. CONCLUSIONS

The first microsecond tomographic facility under construction at the Ballistic Research Laboratory, offers a four orders of magnitude improvement in the time resolution capability over the current generation of scanners (Figure 11). With a spatial resolution of 2 to 4 millimetres on an object of 200 mm, a density resolution of better than 1% and time resolution in the microsecond range, multidimensional density profiles of transient events of ballistic interest will be amenable to study, nonintrusively for the first time. We believe that despite the high source voltages, adequate shielding can be provided against Compton scattering. The facility can also be used for limited-view tomographic cinematography. These conclusions did not consider view limited artifacts and it is recognized that system performance may be degraded under actual firing conditions. It is also interesting to note that the time resolution was obtained without any spatial resolution loss.

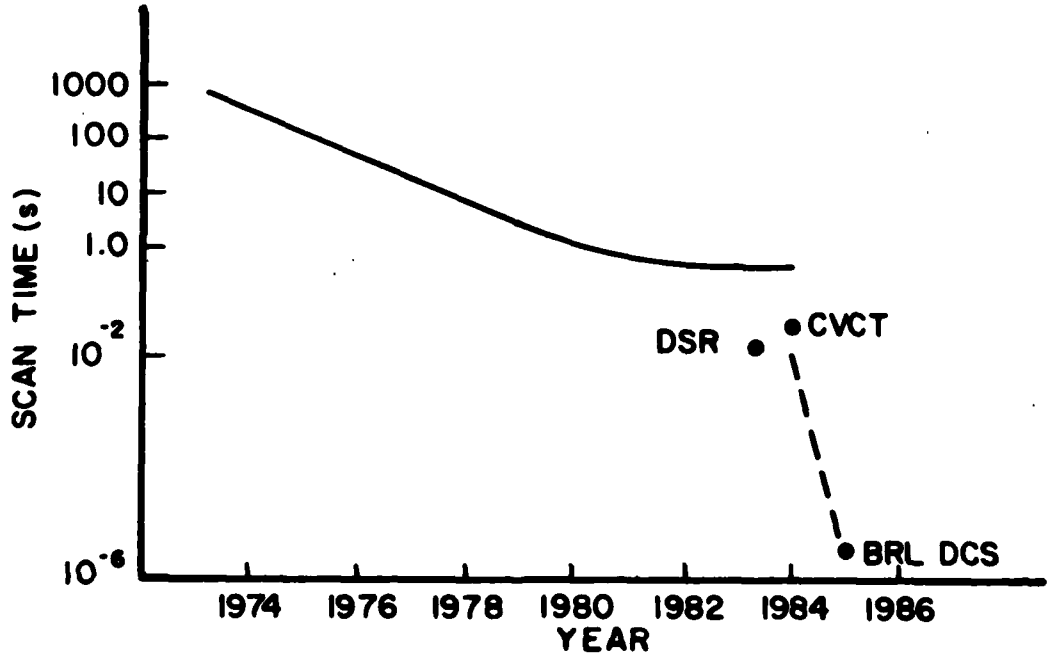

Figure 11. Scan Times of the Current Generation of Scanners.

ACKNOWLEDGMENT

It is a pleasure to thank Dr. G. Minerbo for valuable suggestions on the MENT code methodology as well as Mr. Monte Coleman for his untiring help in implementing the code. Mr. Don McCoy ably assisted in the experiments reported in Section 4.

REFERENCES

1. J.H. Kinsey, R.A. Robb, E.L. Ritman, E.H. Wood, "The DSR- a High Temporal Resolution Volumetric Roentgenographic CT Scanner," Herz, Vol.5, #3, pp. 177-188, 1980.

2. D.W. Farmer, M.J. Lipton, C.B. Higgins, "Cine-CT Captures the Beating Heart," Diagnostic Imaging, Vol.6, pp. 54-58, 1984.

3. J. Trimble, C.L. Aseltine, "Flash X-Ray and Cineradiography at 100 000 Fps," May 1983, ARBRL-TR-02491, Aberdeen Proving Ground, MD, ADA 129090.

4. C.K. Zoltani, K.J. White, R.P. Kruger, "Result of Feasibility Study on Computer Assisted Tomography for Ballistic Applications," August 1983, ARBRL-TR-02513, Aberdeen Proving Ground, MD, ADA 133214.

5. R.A. Brooks, G.H. Glover, A.J. Talbert, R.L. Eisner, F.A. DiBianca, "Aliasing-a Source of Streaks in Computed Tomograms," J. Comput. Assist. Tomography, Vol. 3, #4, 1979, pp. 511-518.

6. T.H. Newton, D.G. Potts, Radiology of the Skull and Brain. Technical Aspects of Computed Tomography, The C.V. Mosby Company, St.Louis, 1981.

7. C.M. Coulam, The Physical Basis of Medical Imaging, Appleton-Century-Crofts, New York, pp. 60, 97, 1981.

8. T.H. Newton and D.G. Potts, (ibid), p. 3931.

9. Anonymous, "CT/T 8800 Technology Brochure, General Electric Medical Systems," 1979; "CT 9800 Evaluation Criteria," General Electric Medical Systems, 1981.

10. F. Jamet, G. Thomer, Flash Radiography, Elsevier Scientific Publishing Co., Amsterdam, 1976.

11. G. Cohen, F.A. DiBianca, "The Use of Contrast-Detail-Dose Evaluation of Image Quality in a Computed Tomographic Scanner," J. Comput. Assist. Tomography, Vol.3, #2, pp. 189-195, 1979.

12. G. Minerbo, "MENT: A Maximum Entropy Algorithm for Reconstructing a Source from Projection Data," Computer Graphics and Image Processing, Vol. 10, pp. 46-68, 1979.

13. J. Skilling, "The Maximum Entropy Method," Nature, Vol. 309, pp. 748-9, 1984.

APPENDIX A.

EQUATIONS FOR SYSTEM GEOMETRIES

APPENDIX A. EQUATIONS FOR SYSTEM GEOMETRIES

The equations for the most compact geometries for Systems II and III are derived here. We begin with System III because the mathematical treatment is simpler. System II requires an iterative solution; it cannot be solved in closed form.

A.1 System III Geometry

Figure 12 shows the basic geometry of System III in its most compact form in which each of two nearly opposite x-ray beams just clear each other's detector. The major variables are:

d_S = source-to-center distance
d_D = detector-to-center distance
d = $2r$ = scan field diameter (largest object)
ϕ = half angle of fan beam
α = half angle between adjacent sources .

By straightforward trigonometry one has:

$$\tan \theta = x \,/\, [\, (d_S + d_D) \sin \phi \,] \qquad \text{(A1)}$$

$$\text{and } x + r \,/\, \cos \theta + d_S = (d_D + d_S) \cos \phi \,. \qquad \text{(A2)}$$

Substituting $\theta = \pi/2 - \phi - \alpha$, combining the above two equations and solving for d_D in terms of d_S, d and N_S gives:

$$d_D = [\, d/2 + d_S \sin (\, \phi + \alpha \,) \,] \,/\, \sin \alpha - d_S \qquad \text{(A3)}.$$

(Here, $\alpha = \pi / N_S$ and $\phi = \arcsin (\, 0.5\, d / d_S \,)$. Further, we note that the number of sources N_S must be odd for a maximally-compact System III. This is not the case for System II.

A.2 System II Geometry

The most compact geometry for System II is given in Figure 13. Here, adjacent detectors must just clear each other. The geometrical variables are defined similarly to those for System III except that α now represents the full-angle between the adjacent sources.

System II geometrical equations are identical to Equations A1 and A2 but now $\theta = \pi / 2 + \phi - \alpha$. Solving for d_D gives:

$$d_D = [d/2 + d_S \sin(\alpha - \phi)] \,/\, \sin(\alpha - 2\phi) - d_S \,. \qquad \text{(A4)}$$

Here, ϕ is defined as it was for System III but a complication arises in the definition of α. For System II, the angle between sources is limited by the necessity that the beams at either end of the source arc clear each other's detectors. This is precisely the constraint arising in System III. Therefore:

$$\alpha_{II} = (\, \pi - \alpha_{III} \,) \,/\, (\, N_S - 1 \,) \qquad \text{(A5)}$$

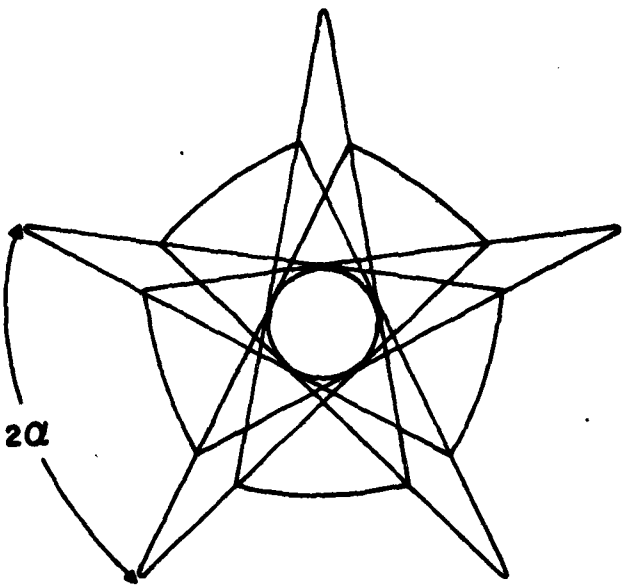

Figure 12. System III Geometry.

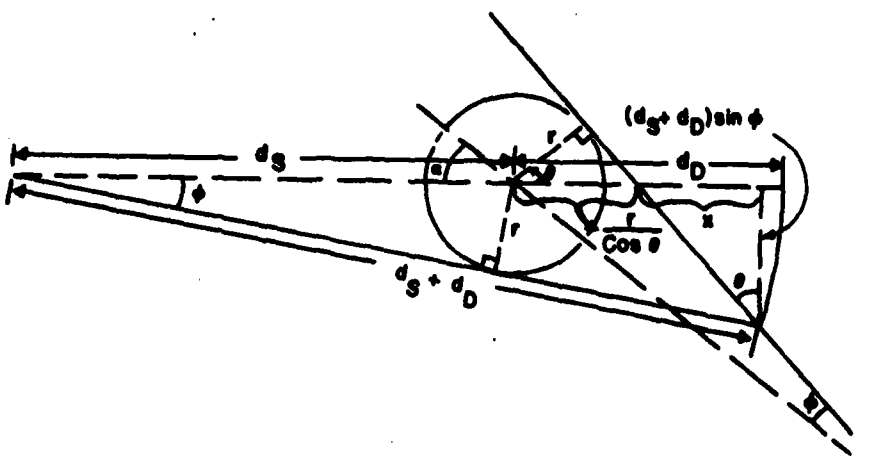

Figure 13. System II Geometry.

where α_{III} is the solution to Equation A3; but d_D is as yet undetermined! Solving Equation A3 for α_{III} gives:

$$\sin\alpha_{II} = [Ad/2+d_S\sin\phi(A^2 - d^2/4+d_S^2\sin^2\phi)^{1/2}]/(A^2+d_S^2\sin^2\phi) \quad (A6)$$

where $A = d_D + d_S(1 - \cos\phi)$. By inspecting trial solutions of the quadratic Equation A6, one finds that the positive square root is correct.

Now we can find d_D for System II by the following iterative procedure:

1. set α_{III} to zero;
2. solve Equation A5 for α_{II};
3. solve Equation A4 for d_D - if converged, go to 5;
4. solve Equation A6 for α_{III} using d_D then loop to 2;
5. finished - record final value for d_D.

Solutions for both system geometries are implemented on an IBM-PC computer in a BASIC program called BRLGEOM which executes in a few seconds.

DISTRIBUTION LIST

No. Of Copies	Organization
12	Administrator Defense Technical Info Center ATTN: DTIC-DDA Cameron Station Alexandria, VA 22304-6145
1	HQ DA DAMA-ART-M Washington, DC 20310
1	Commander USA AMC ATTN: AMCDRA-ST 5001 Eisenhower Avenue Alexandria, VA 22333-0001
1	Commander Armament R&D Center USA AMCCOM ATTN: SMCAR-TSS Dover, NJ 07801
2	Commander Armament R&D Center USA AMCCOM ATTN: SMCAR-TDC Dover, NJ 07801
1	Director Benet Weapons Laboratory Armament R&D Center USA AMCCOM ATTN: SMCAR-LCB-TL Watervliet, NY 12189
1	Commander USA Aviation Research and Development Command ATTN: AMSAV-E 4300 Goodfellow Blvd. St. Louis, MO 63120
1	Director USA Air Mobility Research and Development Laboratory Ames Research Center Moffett Field, CA 94035
6	Commander US Army Research Office ATTN: R. Ghirardelli D. Mann R. Singleton R. Shaw S. Chandra F. Oertel P.O. Box 12211 Research Triangle Park, NC 27709-2211
1	Commander USA Communications - Electronics Command ATTN: AMSEL-ED Fort Monmouth, NJ 07703
1	Commander USA Electronics Research and Development Command Technical Support Activity ATTN: DELSD-L Fort Monmouth, NJ 07703-5301
2	Commander USA AMCCOM ATTN: SMCAR-LCA-G, D.S. Downs J.A. Lannon Dover, NJ 07801
1	Commander USA AMCCOM ATTN: SMCAR-LC-G, S. Harris Dover, NJ 07801
1	Commander USA AMCCOM ATTN: SMCAR-SCA-T, L. Stiefel Dover, NJ 07801
1	Commander USA Missile Command ATTN: AMSMI-R Redstone Arsenal, AL 35898

DISTRIBUTION LIST

No. Of Copies	Organization
1	Commander USA Missile Command ATTN: AMSMI-YDL Redstone Arsenal, AL 35898
2	Commander USA Missile Command ATTN: AMSMI-RK, D.J. Ifshin W. Wharton Redstone Arsenal, AL 35898
1	Commander USA Tank Automotive Command ATTN: AMSTA-TSL Warren, MI 48090
1	Director USA TRADOC Systems Analysis Activity ATTN: ATAA-SL White Sands Missile Range, NM 88002
1	Commander White Sands Missile Range ATTN: STEWS-HP-T White Sands Missile Range, NM 88002
2	Commandant US Army Infantry School ATTN: ATSH-CD-CSO-OR Fort Benning, GA 31905
1	Commander USA Army Development and Employment Agency ATTN: MODE-TED-SAB Fort Lewis, WA 98433
1	*Office of Naval Research* Department of the Navy ATTN: R.S. Miller, Code 432 800 N. Quincy Street Arlington, VA 22217
1	Navy Strategic Systems Project Office ATTN: R.D. Kinert, SP 2731 Washington, DC 20376
1	Commander Naval Air Systems Command ATTN: J. Ramnarace, AIR-54111C Washington, DC 20360
2	Commander Naval Ordnance Station ATTN: C. Irish P.L. Stang, Code 515 Indian Head, MD 20640
2	Commander Naval Ordnance Station ATTN: Code 3023A Dr. C. Dale, 5251F Indian Head, MD 20640
1	*Commander* Naval Surface Weapons Center ATTN: J.L. East, Jr., G-23 Dahlgren, VA 22448
2	Commander Naval Surface Weapons Center ATTN: R. Bernecker, R-13 G.B. Wilmot, R-16 Silver Spring, MD 20910
4	Commander Naval Weapons Center ATTN: R.L. Derr, Code 389 China Lake, CA 93555
2	Commander Naval Weapons Center ATTN: Code 3891, T. Boggs K.J. Graham China Lake, CA 93555

DISTRIBUTION LIST

No. Of Copies	Organization
5	Commander Naval Research Laboratory ATTN: L. Harvey J. McDonald E. Oran J. Shnur R.J. Doyle, Code 6110 Washington, DC 20375
1	Commanding Officer Naval Underwater Systems Center Weapons Dept. ATTN: R.S. Lazar/Code 36301 Newport, RI 02840
1	Superintendent Naval Postgraduate School Dept. of Aeronautics ATTN: D.W. Netzer Monterey, CA 93940
3	Headquarters Ballistic Missile Office ATTN: K.F. Hodge L.C. Farnell D. Lengenfelter Norton Air Force Base San Bernadino, CA 92409
6	AFFTC (DRSC) ATTN: R. Geisler D. George B. Goshgarian J. Levine W. Roe D. Weaver Edwards AFB, CA 93523-5000
2	AFOSR ATTN: L.H. Caveny J.M. Tishkoff Bolling Air Force Base Washington, DC 20332
1	AFWL/SUL Kirtland AFB, NM 87117
2	ARDC ATTN: AMSMC-QAS-A J. Moskowitz J.M. Argento Dover, NJ 07801
1	NASA Langley Research Center ATTN: G.B. Northam/MS 168 Langley Station Hampton, VA 23365
6	National Bureau of Standards ATTN: J. Hastie M. Jacox T. Kashiwagi H. Semerjian S. Ray A.Carasso US Department of Commerce Washington, DC 20234
1	Advanced Research and Applications Corporation ATTN: A.G. Lason 8150 Leesburg Pike Vienna, VA 22190
1	Aerojet Solid Propulsion Co. ATTN: P. Micheli Sacramento, CA 95813
1	Air Force Armament Laboratory ATTN: AFATL/DLODL Eglin AFB, FL 32542-5000
1	Applied Combustion Technology, Inc. ATTN: A.M. Varney P.O. Box 17885 Orlando, FL 32860
1	Argonne National Laboratory Materials Science and Technology Division ATTN: W.A. Ellingson Argonne, IL 60439

DISTRIBUTION LIST

No. Of Copies	Organization
2	Applied Mechanics Reviews The American Society of Mechanical Engineers ATTN: R.E. White A.B. Wenzel 345 E. 47th Street New York, NY 10017
2	Atlantic Research Corp. ATTN: M.K. King 5390 Cherokee Avenue Alexandria, VA 22314
1	Atlantic Research Corp. ATTN: R.H.W. Waesche 7511 Wellington Road Gainesville, VA 22065
1	AVCO Everett Rsch. Lab. Div. ATTN: D. Stickler 2385 Revere Beach Parkway Everett, MA 02149
1	Battelle Memorial Institute Tactical Technology Center ATTN: J. Huggins 505 King Avenue Columbus, OH 43201
1	BDM Corp. ATTN: T.P. Goddard 2600 Cearden Road North Bldg. Monterey, CA 93940
2	Bell Laboratories ATTN: M. Sondhi F. Shepp Murray Hill, NJ 07971
2	Boeing Aerospace Co. Physics Technology Department ATTN: K.D. Friddell A.R. Lowrey Box 3999, M.S. 8C-23 Seattle, WA 98124
2	Exxon Research & Eng. Co. ATTN: A. Dean M. Chou P.O. Box 8 Linden, NJ 07036
1	Ford Aerospace and Communications Corp. DIVAD Division Div. Hq., Irvine ATTN: D. Williams Main Street & Ford Road Newport Beach, CA 92663
1	General Electric Armament & Electrical Systems ATTN: M.J. Bulman Lakeside Avenue Burlington, VT 05401
1	General Electric Company ATTN: A. Wait 2352 Jade Lane Schenectady, NY 12309
1	General Electric Computer Research Medical Diagnostics Systems Program ATTN: T. Kincaid Schenectady, NY 12345
1	General Electric Ordnance Systems ATTN: J. Mandzy 100 Plastics Avenue Pittsfield, MA 01203
1	General Motors Rsch Labs Physics Department ATTN: R. Teets Warren, MI 48090
1	Harry Diamond Laboratories ATTN: DELHD-RT-RD, P.J. Emmerman Adelphi, MD 20438

DISTRIBUTION LIST

No. Of Copies	Organization
1	The Harshaw Chemical Company Crystal and Electronic Products Department ATTN: M.R. Farukhi C. Rozsa Solon, OH 44139
3	Hercules, Inc. Allegany Ballistics Lab. ATTN: R.R. Miller P.O. Box 210 Cumberland, MD 21501
3	Hercules, Inc. Bacchus Works ATTN: K.P. McCarty P.O. Box 98 Magna, UT 84044
1	Hercules, Inc. AFATL/DLDL ATTN: R.L. Simmons P.O. Box 1646 Eglin AFB, FL 32542
3	Hewlett-Packard Corp. ATTN: F. Charbonnier L. Bailey A. Kennedy 1700 South Baker Street McMinnville, OR 97128
1	Honeywell, Inc. Defense Systems Division ATTN: D.E. Broden/ MS MN50-2000 600 2nd Street NE Hopkins, MN 55343
1	Hughes Aircraft Company ATTN: T.E. Ward 8433 Fallbrook Avenue Canoga Park, CA 91303
1	IBM Corporation ATTN: A.C. Tam Research Division 5600 Cottle Road San Jose, CA 95193
1	Industrial Quality, Inc. ATTN: H. Berger P.O. Box 2397 Gaithersburg, MD 20879
1	Director Lawrence Livermore National Laboratory ATTN: C. Westbrook P.O. Box 808 Livermore, CA 94550
1	Director Lawrence Livermore National Laboratory ATTN: M. Costantino P.O. Box 808 Livermore, CA 94550
1	Director Lawrence Livermore National Laboratory ATTN: A. Buckingham P.O. Box 808 Livermore, CA 94550
1	Director Lawrence Livermore National Laboratory ATTN: Library P.O. Box 808 Livermore, CA 94550
1	Lockheed Missiles & Space Co. ATTN: George Lo 3251 Hanover Street Dept. 52-35/B204/2 Palo Alto, CA 94304
3	Los Alamos National Lab ATTN: B. Nichols T7, MS-B284 C. Mader K. Hanson P.O. Box 1663 Los Alamos, NM 87545

DISTRIBUTION LIST

No. Of Copies	Organization
1	Massachusetts Institute of Technology Laboratory for Information and Decision Systems ATTN: A.S. Willsky Cambridge, MA 02139
2	Mathematics Research Center ATTN: B. Noble J. Nohel 610 Walnut Street Madison, WI 53706
3	Mayo Clinic Biodynamics Research Unit ATTN: E.L. Ritman J.H. Kinsey R.A. Robb 200 First Street, S.W. Rochester, MN 55901
1	MCI Optonix, Inc. ATTN: G. Zweig Horsehill Road P.O. Box 1 Cedar Knolls, NJ 07927
1	Mirror Electronics Company ATTN: R.P. Espejo P.O. Box 206 Gaston, OR 97119-0206
1	Dr. G. Morgan 1912 Sheffield Court Severn, MD 21144
1	Naval Coastal Systems Center Code 2210-C ATTN: J. Mittleman Panama City, FL 32407
1	Olin Corporation Smokeless Powder Operations ATTN: R.L. Cook P.O. Box 222 St. Marks, FL 32355
1	Paul Gough Associates, Inc. ATTN: P.S. Gough P.O. Box 1614 1048 South Street Portsmouth, NH 03801
2	Princeton Combustion Research Laboratories, Inc. ATTN: M. Summerfield N.A. Messina 475 US Highway One Monmouth Junction, NJ 08852
1	Princeton Scientific Instruments, Inc. ATTN: J.L. Lowrance P.O. Box 252 Kingston, NJ 08528
1	Rockwell International Corp. Rocketdyne Division ATTN: J.E. Flanagan/HB02 6633 Canoga Avenue Canoga Park, CA 91304
1	SAI ATTN: N. Banks 626 Town Ct. Dr. Joppa, MD 21085
3	Sandia National Laboratories Combustion Sciences Dept. ATTN: R. Cattolica D. Stephenson P. Mattern Livermore, CA 94550
1	Sandia National Laboratories ATTN: M. Smooke Division 8353 Livermore, CA 94550
1	Science Applications, Inc. ATTN: R.B. Edelman 23146 Cumorah Crest Woodland Hills, CA 91364

DISTRIBUTION LIST

No. Of Copies	Organization
1	Science Applications, Inc. ATTN: H.S. Pergament 1100 State Road, Bldg. N Princeton, NJ 08540
1	Scientific Research Associates, Inc. ATTN: H. McDonald P.O. Box 498 Glastonbury, CT 06033
1	Shell Development Oil Co. ATTN: Dr. H. Vinegar P.O. Box 481 Houston, TX 77001
4	SRI International ATTN: G. Smith D. Crosley D. Golden 333 Ravenswood Avenue Menlo Park, CA 94025
1	Stevens Institute of Tech. Davidson Laboratory ATTN: R. McAlevy, III Hoboken, NJ 07030
1	Teledyne McCormack-Selph ATTN: C. Leveritt 3601 Union Road Hollister, CA 95023
1	Thiokol Corporation Elkton Division ATTN: W.N. Brundige P.O. Box 241 Elkton, MD 21921
3	Thiokol Corporation Huntsville Division ATTN: R. Glick Huntsville, AL 35807
1	Thiokol Corporation Wasatch Division P.O. Box 524 Brigham City, UT 84302
1	Thorn EMI Gencom, Inc. ATTN: L.M. Lieberman 80 Express Street Plainview, NY 11803
1	United Technologies ATTN: A.C. Eckbreth East Hartford, CT 06108
2	Chemical Systems Director United Technologies ATTN: R.S. Brown R.O. McLaren P.O. Box 358 Sunnyvale, CA 94086
1	Universal Propulsion Company ATTN: H.J. McSpadden Black Canyon Stage 1 Box 1140 Phoenix, AZ 85029
1	Veritay Technology, Inc. ATTN: E.B. Fisher 4845 Millersport Highway P.O. Box 305 East Amherst, NY 14051-0505
1	University of Arizona Optical Sciences Center ATTN: B. Roy Prieden Tucson, AZ 85721
1	Brigham Young University Dept. of Chemical Engineering ATTN: M.W. Beckstead Provo, UT 84601
1	California Institute of Tech. Jet Propulsion Laboratory ATTN: MS 125/159 4800 Oak Grove Drive Pasadena, CA 91103

DISTRIBUTION LIST

No. Of Copies	Organization
1	California Institute of Technology ATTN: F.E.C. Culick/ MC 301-46 204 Karman Lab. Pasadena, CA 91125
1	University of California, Berkeley Mechanical Engineering Dept. ATTN: J. Daily Berkeley, CA 94720
1	University of California Donner Laboratory ATTN: T.F. Budinger Berkeley, CA 94720
1	University of California Los Alamos National Lab. ATTN: T.D. Butler P.O. Box 1663, Mail Stop B216 Los Alamos, NM 87545
1	University of California, San Diego Energy Center and Dep. Applied Mechanics ATTN: S.S. Penner La Jolla, CA 92093
2	University of California, Santa Barbara Quantum Institute ATTN: K. Schofield M. Steinberg Santa Barbara, CA 93106
1	University of Southern California Dept. of Chemistry ATTN: S. Benson Los Angeles, CA 90007
1	Case Western Reserve Univ. Div. of Aerospace Sciences ATTN: J. Tien Cleveland, OH 44135
1	Cornell University Department of Chemistry ATTN: E. Grant Baker Laboratory Ithaca, NY 14853
1	Univ. of Dayton Rsch Inst. ATTN: D. Campbell AFRPL/PAP Stop 24 Edwards AFB, CA 93523
1	University of Florida Dept. of Chemistry ATTN: J. Winefordner Gainesville, FL 32611
1	George Washington University School of Engineering and Applied Science ATTN: R. Goulard Washington, DC 20052
5	Georgia Institute of Technology School of Aerospace Engineering ATTN: E. Price W.C. Strahle B.T. Zinn Atlanta, GA 30332
2	University of Illinois Dept. of Mech. Eng. ATTN: H. Krier S.L. Soo 1206 W. Green St. Urbana, IL 61801
1	Johns Hopkins University/APL Chemical Propulsion Information Agency ATTN: T.W. Christian Johns Hopkins Road Laurel, MD 20707

DISTRIBUTION LIST

No. Of Copies	Organization
1	University of Michigan Department of Mechanical Engineering ATTN: C.M. Vest Ann Arbor, MI 48104
1	University of Minnesota Dept. of Mechanical Engineering ATTN: E. Fletcher Minneapolis, MN 55455
3	University of North Carolina Bio-Medical Engineering Department ATTN: F.A. DiBianca Chapel Hill, NC 27514
1	Oregon State University Department of Mathematics ATTN: K. Smith Corvallis, OR 97331
1	Hospital of the University of Pennsylvania Department of Radiology ATTN: G.T. Herman 3400 Spruce Street Philadelphia, PA 19104
4	Pennsylvania State University Applied Research Laboratory ATTN: G.M. Faeth K.K. Kuo H. Palmer M. Micci University Park, PA 16802
1	University of Pittsburgh ATTN: D. Sashin Pittsburgh, PA 15261
1	Polytechnic Institute of NY ATTN: S. Lederman Route 110 Farmingdale, NY 11735
2	Princeton University Forrestal Campus Library ATTN: K. Brezinsky I. Glassman P.O. Box 710 Princeton, NJ 08540
1	Princeton University MAE Dept. ATTN: F.A. Williams Princeton, NJ 08544
1	Purdue University School of Aeronautics and Astronautics ATTN: J.R. Osborn Grissom Hall West Lafayette, IN 47907
2	Purdue University School of Mechanical Engineering ATTN: N.M. Laurendeau S.N.B. Murthy TSPC Chaffee Hall West Lafayette, IN 47906
1	Rensselaer Polytechnic Inst. Dept. of Chemical Engineering ATTN: A. Fontijn Troy, NY 12181
1	Stanford University Dept. of Mechanical Engineering ATTN: R. Hanson Stanford, CA 94305
1	Stanford University Department of Physics ATTN: A. Macovski Palo Alto, CA 94305
1	University of Texas Dept. of Chemistry ATTN: W. Gardiner Austin, TX 78712

DISTRIBUTION LIST

No. Of Copies	Organization
1	University of Utah Dept. of Chemical Engineering ATTN: G. Flandro Salt Lake City, UT 84112
1	University of Utah Department of Mathematics ATTN: F. Stenger Salt Lake City, UT 84112
2	Virginia Polytechnic Institute and State University ATTN: J.A. Schetz R.T. Smith Blacksburg, VA 24061
1	Washington University Mallinckrodt Institute of Radiology ATTN: M.W. Vannier 510 S. Kings Highway St. Louis, MO 63110

No. Of Copies	Organization
	Aberdeen Proving Ground
	Dir, USAMSAA ATTN: AMXSY-D AMXSY-MP, H. Cohen
	Cdr, USATECOM ATTN: AMSTE-TO-F
	Cdr, CRDC, AMCCOM ATTN: SMCCR-RSP-A SMCCR-MU SMCCR-SPS-IL

USER EVALUATION SHEET/CHANGE OF ADDRESS

This Laboratory undertakes a continuing effort to improve the quality of the reports it publishes. Your comments/answers to the items/questions below will aid us in our efforts.

1. BRL Report Number_____ Date of Report_____

2. Date Report Received_____

3. Does this report satisfy a need? (Comment on purpose, related project, or other area of interest for which the report will be used.)_____

4. How specifically, is the report being used? (Information source, design data, procedure, source of ideas, etc.)_____

5. Has the information in this report led to any quantitative savings as far as man-hours or dollars saved, operating costs avoided or efficiencies achieved, etc? If so, please elaborate._____

6. General Comments. What do you think should be changed to improve future reports? (Indicate changes to organization, technical content, format, etc.)

CURRENT ADDRESS

Name

Organization

Address

City, State, Zip

7. If indicating a Change of Address or Address Correction, please provide the New or Correct Address in Block 6 above and the Old or Incorrect address below.

OLD ADDRESS

Name

Organization

Address

City, State, Zip

(Remove this sheet along the perforation, fold as indicated, staple or tape closed, and mail.)

— — — — — — — — — — FOLD HERE — — — — — — — — — —

Director
US Army Ballistic Research Laboratory
ATTN: AMXBR-OD-ST
Aberdeen Proving Ground, MD 21005-5066

NO POSTAGE
NECESSARY
IF MAILED
IN THE
UNITED STATES

OFFICIAL BUSINESS
PENALTY FOR PRIVATE USE, $300

BUSINESS REPLY MAIL
FIRST CLASS PERMIT NO 12062 WASHINGTON, DC
POSTAGE WILL BE PAID BY DEPARTMENT OF THE ARMY

Director
US Army Ballistic Research Laboratory
ATTN: AMXBR-OD-ST
Aberdeen Proving Ground, MD 21005-9989

— — — — — — — — — — FOLD HERE — — — — — — — — — —

END

FILMED

10-85

DTIC